# Changes in spin and lattice dynamics induced by magnetic and structural phase transitions in multiferroic $SrMn_7O_{12}$

Stanislav Kamba,[1,*] Veronica Goian,[1] Filip Kadlec,[1] Dmitry Nuzhnyy,[1] Christelle Kadlec,[1] Jakub Vít,[1,2,3] Fedir Borodavka,[1] Iana S. Glazkova,[4] and Alexei A. Belik[5]

[1]*Institute of Physics, Czech Academy of Sciences, Na Slovance 2, 182 21 Prague 8, Czech Republic*
[2]*Faculty of Nuclear Science and Physical Engineering, Czech Technical University, Břehová 7, 115 19 Prague 1, Czech Republic*
[3]*Department of Physics, Budapest University of Technology and Economics, H-1111 Budapest, Hungary*
[4]*Department of Chemistry, Lomonosov Moscow State University, Leninskie Gory, 119992 Moscow, Russia*
[5]*Research Center for Functional Materials, National Institute for Materials Science (NIMS), Namiki 1-1, Tsukuba, Ibaraki 305-0044, Japan*

(Received 11 February 2019; revised manuscript received 3 May 2019; published 20 May 2019)

$SrMn_7O_{12}$ is a recently synthesized homolog of multiferroic $CaMn_7O_{12}$. Upon cooling, $SrMn_7O_{12}$ undergoes a series of structural and magnetic phase transitions from cubic to rhombohedral symmetry, and to an incommensurately modulated crystal structure, which is connected with charge and orbital ordering of the Mn cations. We report infrared, terahertz, and Raman spectra of $SrMn_7O_{12}$ ceramics reflecting corresponding changes in phonon selection rules, including new phonons appearing in spin-order-induced ferroelectric phases. The observed phonon activities are compared with the predictions from the factor-group analysis. In the high-temperature phase, more phonons are observed than the number predicted for the cubic symmetry. This is explained by the presence of rhombohedral clusters in the cubic phase. The strongest variations occur in THz spectra near the two magnetic phase transitions, at $T_{N1} = 87$ K and $T_{N2} = 63$ K. These activate new modes in the spectra, with resonance frequencies and intensities changing with temperature and magnetic field. Below $T_{N2}$, we observed a transfer of oscillator strengths from low-frequency phonons to these excitations, which we assign to electromagnons.

DOI: 10.1103/PhysRevB.99.184108

In the last years, the quadruple perovskite $CaMn_7O_{12}$ has raised great interest among the researchers involved in multiferroics. This is due to its unusual symmetry, and to the fact that this compound exhibits one of the highest values of spontaneous ferroelectric (FE) polarization among all spin-order-induced ferroelectrics [1,2], which could be interesting for potential applications. The origin of the high polarization was the subject of numerous theoretical studies with sometimes controversial results [3,4]. Recently, an agreement was found that the polarization arises from an interplay between the inverse Dzyaloshinskii-Moriya interaction, which stabilizes a helicoidal spin structure, and the exchange striction, which induces the large polarization [3–7]. The multiferroicity can also be explained by a ferroaxial coupling of the magnetic chirality to the macroscopic structural rotations associated with the rhombohedral structure [2,3].

$CaMn_7O_{12}$ can be regarded as a kind of perovskite with a quadruple unit cell; its formula can also be written as $(CaMn_3)Mn_4O_{12}$. At high temperatures, its structure is cubic (space group $Im\bar{3}$), where four $B$-site Mn cations have a mixed valency of 3.25, and the system is conducting. At $T_{co} = 462$ K, Mn undergoes charge ordering, whereby $(CaMn_3)Mn_3{}^{3+}Mn^{4+}O_{12}$ transforms to an insulating rhombohedral $R\bar{3}$ phase [8]. Additional orbital ordering of Mn cations occurs at $T_{oo} = 258$ K, inducing a structural incommensurate modulation with a propagation vector $q_c = (0, 0, 2.077)$ [9]. At $T_{N1} = 91$ K, an antiferromagnetic helicoidal structure appears; it is again incommensurately modulated along the $c$ axis with $q_m = (0, 0, 1.0394)$ [9–11]. Finally, below $T_{N2} = 48$ K, the magnetic structure exhibits two modulations with the corresponding propagation vectors $q_{m1}$ and $q_{m2}$, where $2q_m = q_{m1} + q_{m2}$. FE polarization appears at $T_{N1}$ and saturates [2] below $T_{N2}$ at a record high value of 2870 $\mu Cm^{-2}$. However, a more recent study questioned this value [12].

Earlier studies of $CaMn_7O_{12}$ using infrared (IR) and Raman spectroscopies reported noticeable phonon splitting at $T_{co}$ and $T_{oo}$ due to changes in selection rules [13–15]. Moreover, above $T_{oo}$, inelastic x-ray scattering revealed an anomalous softening of a phonon with a wave vector corresponding to the modulation of the incommensurate phase below $T_{oo}$ [16]. The same phonon becomes Raman active in the incommensurate phase, where the Brillouin zone (BZ) is folded and the phonon moves to the BZ center [17]. Below $T_{N1}$, two spin excitations were observed in far-IR and THz studies; these modes become more pronounced on cooling below $T_{N2}$, and they split in external magnetic field [13]. Since the oscillator strengths of some polar phonons are transferred to magnons, it was proposed that these excitations are electromagnons [13]. This idea is supported by recent work revealing the same excitations in Raman spectra [18], because in the polar FE phases, electromagnons should be both IR and Raman active [19].

Recently, it was reported that $AMn_7O_{12}$ ($A$ = Sr, Cd, Pb) exhibit a sequence of structural and magnetic phase transitions analogous to that in $CaMn_7O_{12}$. With increasing radius of the

*Corresponding author: kamba@fzu.cz

 

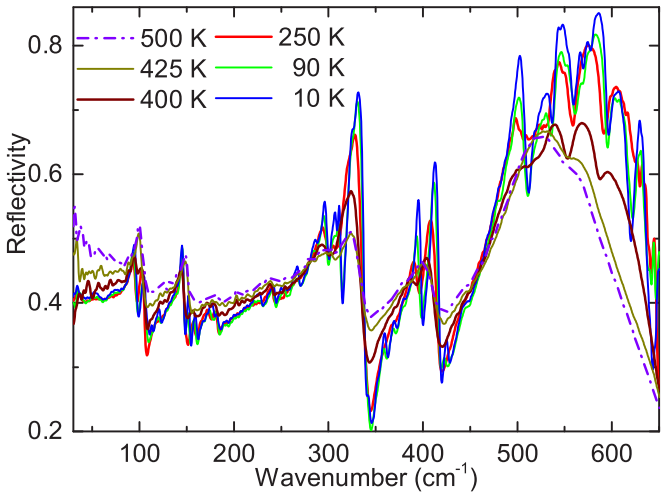


FIG. 1. Temperature dependence of IR reflectivity spectra of $SrMn_7O_{12}$ ceramics.

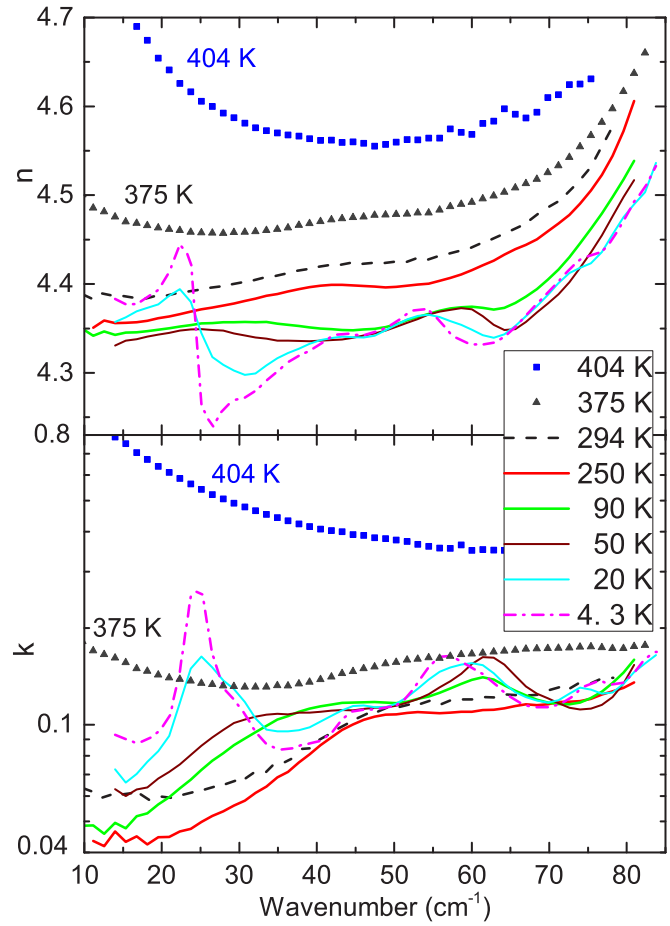


FIG. 2. Temperature dependence of complex refractive index of $SrMn_7O_{12}$ ceramics obtained by THz time-domain spectroscopy.

*A*-site cations, the values of $T_{co}$ decrease, whereas those of $T_{oo}$ and $T_{N2}$ increase, and $T_{N1}$ remains approximately constant in the range 80–90 K [8,11,12,20]. The spin and lattice dynamics of $AMn_7O_{12}$ ($A$ = Sr, Cd, Pb) still need to be investigated. In this paper, we focus on $SrMn_7O_{12}$ and we show how its phonons and spin-wave excitations evolve with temperature and magnetic field. The results are discussed based on phonon and magnon selection rules in various crystal and magnetic phases.

$SrMn_7O_{12}$ was prepared from a stoichiometric mixture of $Mn_2O_3$ and $4H$-$SrMnO_3$, placed in a Au capsule and treated for 2 h at 6 GPa and 1573 K in a belt-type high-pressure apparatus. The heating rate to achieve the above temperature was set to 10 K/min. After the heat treatment, the samples were quenched to room temperature and the pressure was slowly released. More details about the sample preparation can be found elsewhere [8]. The ceramic pellets with a diameter of ca. 5 mm and 1 mm thick were optically polished; for THz studies, they were thinned down to a thickness of 350 $\mu$m.

IR reflectivity was measured using the Fourier-transform IR spectrometer Bruker IFS113v. Time-domain THz transmission studies were performed using two custom-made spectrometers, and micro-Raman spectra were obtained using a Renishaw RM 1000 spectrometer. Details about the experimental techniques used can be found elsewhere [13,21].

Figure 1 shows IR spectra of the $SrMn_7O_{12}$ ceramics at selected temperatures. One can see an abrupt splitting and sharpening of all reflection bands below $T_{co} = 404$ K. On cooling, the reflection band intensities increase due to lowering phonon damping. The low-frequency reflectivity level below 100 cm$^{-1}$ gradually decreases on cooling due to the transition from a metallic to insulating phase at $T_{co}$.

The spectra below 80 cm$^{-1}$ were measured also using time-domain THz spectroscopy, yielding spectra of the complex index of refraction $N(\omega) = n(\omega) + ik(\omega)$ (Fig. 2). The THz and IR spectra were fitted together using a sum of harmonic oscillators describing phonons and spin excitations, and a Drude term expressing free-carrier conductivity [19] (see the calculated complex permittivity spectra in Fig. S1 in the Supplemental Material [22]). Above 400 K, the $n(\omega)$ and $k(\omega)$ spectra are smooth due to the conductivity in the cubic phase. At lower temperatures, the sample becomes insulating and phonons and magnons gradually activate in the THz spectra on cooling—see Figs. 2 and 3. Below $T_{co} = 404$ K, a broad phonon activates near 75 cm$^{-1}$, and its frequency softens towards $T_{oo} = 265$ K. Below $T_{oo}$, the phonon splits in two components which soften slightly as the temperature drops towards $T_{N1} = 87$ K. Figure 3(b) shows the plasma frequencies $\Omega_j = \sqrt{\Delta\varepsilon_j}\omega_j$ of the modes obtained from the fits, where $\Delta\varepsilon_j$ and $\omega_j$ mark the dielectric strength and resonance frequency of the $j$th mode, respectively. At $T_{oo}$, one can see a sudden drop in $\Omega_2$ which is compensated by the value of $\Omega_1 \approx 20$ cm$^{-1}$ of the newly appearing phonon. This is in agreement with the sum rule $\sum_j \Omega_j = \text{const}(T)$ [23] and reveals coupling between these two phonons, which is further confirmed by the gradual decrease in $\Omega_2$ and increase in $\Omega_1$ upon further cooling towards $T_{N2}$.

The main changes in THz spectra occur below $T_{N2} = 63$ K, when five new modes activate (see open symbols in Fig. 3). At the same time, the phonon plasma frequencies $\Omega_1$, $\Omega_2$, and $\Omega_3$ decrease on cooling. This is a clear sign of a transfer of dielectric strength to these modes, so at least a part of the modes are polar phonons or electromagnons. Their activation at $T_{N2}$ may be due to the fact that the system becomes FE (i.e.,

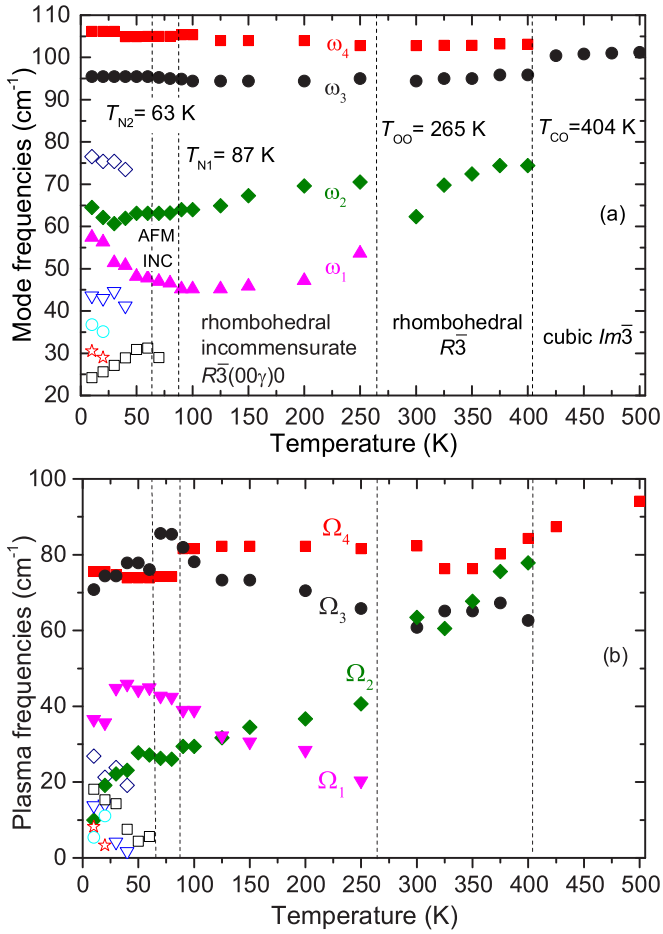


FIG. 3. (a) Temperature dependence of the low-frequency excitations observed in THz and IR spectra of $SrMn_7O_{12}$. The open symbols correspond to spin excitations or phonons activated by breaking of the inversion center, whereas the remaining phonons are marked by solid symbols. (b) Temperature dependence of the mode plasma frequencies $\Omega_j = \sqrt{\Delta\varepsilon_j}\omega_j$. The symbols correspond to those used for the modes in (a).

acentric) only below $T_{N2}$, as proposed by Terada *et al.* [12]. Alternatively, the crystal may become FE already at $T_{N1}$, in which case, at temperatures between $T_{N2}$ and $T_{N1}$, the FE order parameter would be too small for the new modes to appear in the spectra. Note that some modes exhibit anomalies near 30 K, as much as 30 K below $T_{N2}$, which might indicate another magnetic phase transition. Note also the strong increase in $\omega_1$ below $T_{N1}$, evidencing a strong spin-phonon coupling.

For a better resolution of the mode splitting below phase transitions, Fig. S3a in the Supplemental Material [22] shows in detail the experimental THz spectra together with their fits using a sum of Lorentz oscillators. It is worth noting that in the reflectivity spectra, all THz modes are much weaker than the phonons above 90 cm$^{-1}$. This can be seen in Fig. S3b in the Supplemental Material [22].

THz spectra in external magnetic field of up to 7 T at different temperatures were measured in the Voigt configuration. Below $T_{N2}$, small reproducible changes were observed (see Fig. 4). For example, at 10 K, a mode appears near 15 cm$^{-1}$ and its intensity increases with magnetic field. Further, with increasing magnetic field, the modes near 24, 28, and 45 cm$^{-1}$ become weaker [see Fig. 4(a)] and the mode near 55 cm exhibits a blueshift to 58 cm$^{-1}$. With increasing temperature, the changes in the THz spectra due to the magnetic field decrease, but they are still distinct [see Figs. 4(b) and 4(c)]. All these changes demonstrate that these modes are most probably spin excitations. Since, upon cooling, at least some of them receive dielectric strength from the polar phonons, they can be quite reliably assigned to electromagnons. Unfortunately, we do not dispose of a single crystal which would allow for measurements of polarized spectra or directional dichroism, in order to determine which of the magnetic excitations are magnons or electromagnons. It is worth noting that similar THz excitations were observed also in $CaMn_7O_{12}$. In that case, the observed mode shifts and splittings due to the magnetic field were more pronounced, because the spectra were measured up to 12 T [13].

Figure 5 presents Raman scattering spectra, revealing phonon lines gradually developing on cooling. Surprisingly, only one new phonon activates below the metal-insulator phase transition (404 K) where the structure changes from cubic to rhombohedral; this will be discussed below. Other modes activate in the incommensurate phase below $T_{oo}$ due to the folding of phonons out of the BZ center. On cooling, the intensity of most of the modes increases due to a reduced damping. We did not observe any spin excitations below 50 cm$^{-1}$ known from THz spectra, but we cannot exclude their existence. Note that various authors investigated Raman spectra of the homologous $CaMn_7O_{12}$ ceramics [13,14,17] without observing any spin excitations, although these were recently reported in the $CaMn_7O_{12}$ single crystal [18]. The absence of magnetic modes in the Raman spectra of ceramics is probably caused by their low intensities and also by the dependence of the spectra on the orientation of the incident light with respect to the ceramic grains.

Next, we compare the observed numbers of phonons with results of the factor-group analysis of BZ-center phonons. In the high-temperature cubic phase we obtained the following phonon counts, symmetries, and activities in IR and Raman (R) spectra [13,14,24],

$$\begin{aligned}\Gamma_{Im\bar{3}} = {} & 12F_u(x) + 2A_u(-) + 2E_u(-) \\ & + 2A_g(x^2+y^2+z^2) + 4F_g(xy, xz, yz) \\ & + 2E_g(x^2+y^2-z^2, \sqrt{3}x^2-\sqrt{3}y^2). \end{aligned} \quad (1)$$

In the unmodulated rhombohedral $R\bar{3}$ structure we obtained

$$\begin{aligned}\Gamma_{R\bar{3}} = {} & 14E_u(x,y) + 14A_u(z) + 6A_g(x^2+y^2, z^2) \\ & + 6E_g(x^2-y^2, xy, yz, xz). \end{aligned} \quad (2)$$

Thus, after subtraction of acoustic modes, 11 (8) and 26 (12) IR- (Raman-) active modes can be expected in the cubic and rhombohedral structures, respectively. Below $T_{oo}$, the structure becomes incommensurately modulated [superspace group $R\bar{3}(00\gamma)0$]. This may activate additional phonons with wave vectors corresponding to the modulation wave vector, so the number of phonons increases again.

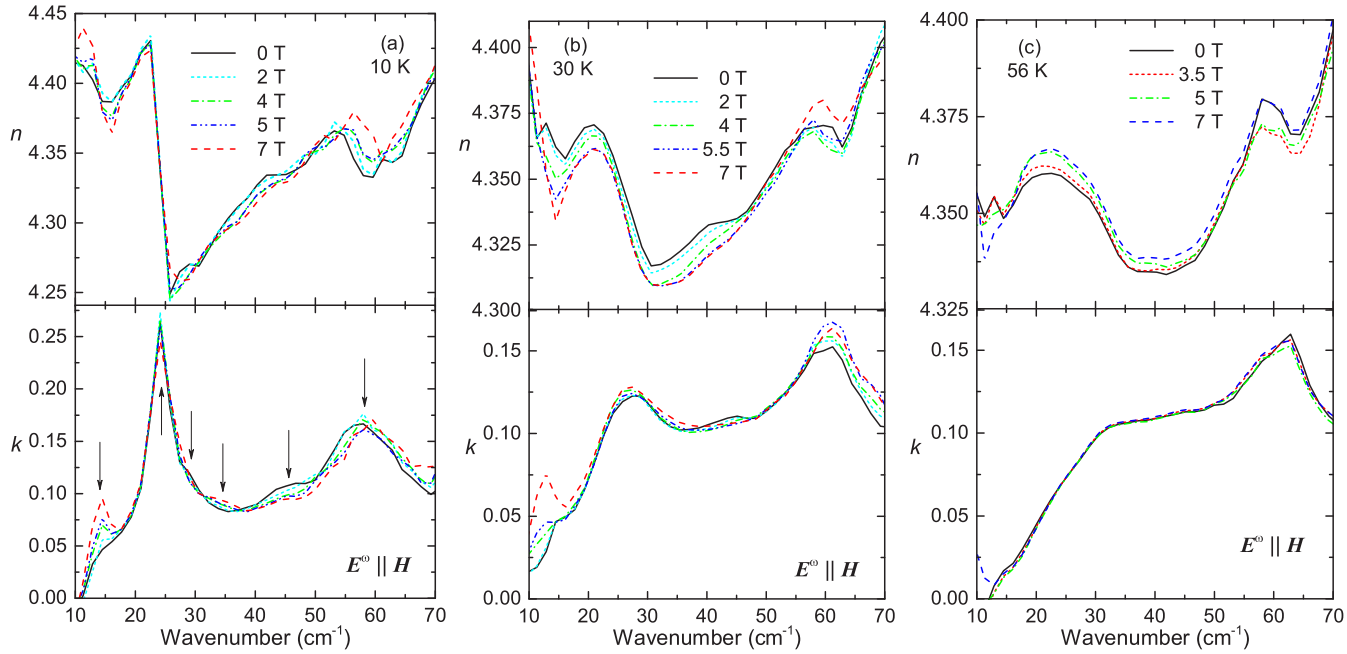


FIG. 4. Magnetic field dependence of complex refractive index of $SrMn_7O_{12}$ ceramics at selected temperatures. At 10 K, the mode frequencies are marked by arrows. The spectra were measured in the Voigt geometry, where the electric vector $\mathbf{E}^{\omega}$ of the THz beam was parallel to external magnetic field $\mathbf{H}$. The $\mathbf{E}^{\omega} \perp \mathbf{H}$ spectra (not shown) were the same within the experimental error.

In the magnetic phases, $SrMn_7O_{12}$ crystallizes in the $R31'(00\gamma)ts$ incommensurate magnetic superspace group [10,11] which is polar, i.e., it allows the FE ordering. The magnetic point group $31'$ does not belong to the 58 black and white Shubnikov point groups, so the phonon selection rules cannot be influenced by the magnetic ordering [25]. If we neglect the structural and magnetic modulations, the structure is polar ($R3$) and the phonons should have the following symmetries and activities [24],

$$\Gamma_{R3} = 20A(z, x^2 + y^2, z^2) + 20E(x, y, x^2 - y^2, xy, yz, xz). \tag{3}$$

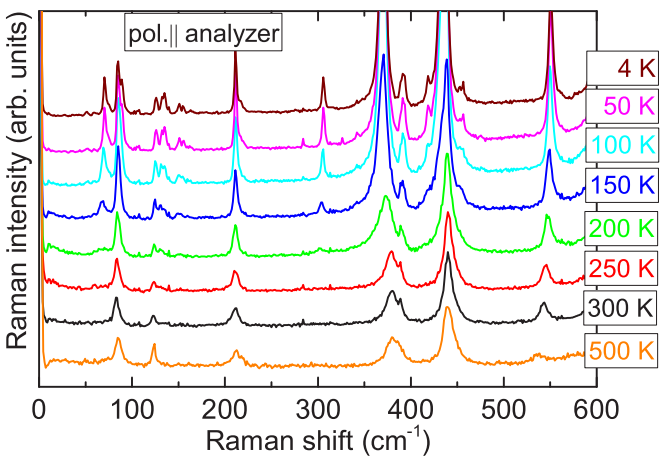


FIG. 5. Temperature dependence of Raman scattering spectra of $SrMn_7O_{12}$ ceramics with the parallel polarizer and analyzer.

Thus, after subtracting two acoustic modes, 38 of both IR- and Raman-active modes can be expected in the unmodulated $R3$ multiferroic phase. In polar structures, electromagnons follow the same selection rules as phonons, so, in the present case, they should be both IR and Raman active.

We have observed 16, 25, 40, and 49 IR-active modes in the cubic, rhombohedral, incommensurate, and magnetic phases (at 10 K), respectively (see the temperature evolution of all mode frequencies in Fig. S2 [22]). In the Raman spectra (Figs. 5 and S4 [22]), we resolved nine phonons in the cubic phase, ten modes in the unmodulated rhombohedral phase at 300 K, and 22 modes at 10 K (i.e., in the multiferroic phase). The main discrepancy occurs in the cubic phase where we observed five (one) IR- (Raman-) active modes in excess. These might originate in multiphonon absorption, but since these modes were observed also in the low-temperature phases, we believe they appear due to rhombohedral nanoregions embedded in the cubic phase. Note that in $CaMn_7O_{12}$, a coexistence of cubic and rhombohedral phases 40 K above $T_{co}$ was identified using x-ray diffraction and neutron powder diffraction [26]. In contrast, IR spectroscopy is more sensitive to local symmetry breaking than the diffraction methods [27], which explains that the additional modes were observed in $SrMn_7O_{12}$ even 100 K above $T_{co}$.

In the rhombohedral phase we observed only one IR phonon less and two Raman modes less than predicted [see Eq. (2)]. This corresponds very well to the $R\bar{3}$ structure; the few missing modes most likely have low intensities, or they may overlap with other modes. Exactly the same number of Raman-active phonons (ten out of the 12 allowed) were observed in the rhombohedral phase of $CaMn_7O_{12}$ [14]. Also in the IR spectra of $CaMn_7O_{12}$, the number of phonons

appropriate to the rhombohedral phase (25 out of predicted 26 modes) were observed [13]. The appearance of additional 15 IR-active and 12 Raman-active modes below $T_{oo}$ in $SrMn_7O_{12}$ corresponds to the loss of translation symmetry along the $c$ axis, which leads to the activation of phonons out of the BZ center. Five out of the nine additional IR-active modes newly activated in the magnetic phases are most probably spin excitations (at 10 K, they are seen at 25, 29, 36, 58, and 76 $cm^{-1}$—see Fig. 3 and Fig. S3 in the Supplemental Material [22]). Four additional phonons activate above 110 $cm^{-1}$ due to the symmetry lowering in the spin-induced FE phase, where the originally Raman-active modes become also IR active (see the temperature dependence of the frequencies of all IR-active modes in Fig. S2 [22]). A similar dramatic increase of phonon activities with lowering temperature was observed in the IR and Raman spectra of $CaMn_7O_{12}$ [13,14,18].

In conclusion, we have measured the Raman and IR spectra of $SrMn_7O_{12}$ ceramics at varying temperatures, as well as THz spectra at different temperatures and in external magnetic fields. In the high-temperature cubic phase, the IR spectra contain five more modes than predicted by the theory which we explain by the existence of embedded rhombohedral nanoregions above $T_{co}$. By contrast, in the rhombohedral phase, the number of observed phonons corresponds to the factor-group analysis. Additional phonons activate in IR and Raman spectra in the incommensurately modulated phase, which can be explained by the breaking of translational symmetry below $T_{oo}$.

In the multiferroic phases, at 10 K, on the one hand, Raman spectra revealed only 22 out of 38 phonons predicted by the factor-group analysis. The absent modes are probably too weak, or they may overlap with other stronger modes. On the other hand, 49 IR-active modes were observed, 11 more than the 38 ones allowed in the $R3$ structure. Apparently, some of the extra modes are off-BZ-center phonons activated by the incommensurate modulation. However, many of the excess modes observed in the THz spectra are sensitive to magnetic field, which is typical of spin excitations. Since these modes receive oscillator strengths from polar phonons, they are most probably electromagnons.

This work was supported by the Czech Science Foundation Project No. 18-09265S and the Operational Programme Research, Development and Education financed by European Structural and Investment Funds and the Czech Ministry of Education, Youth and Sports (Project No. SOLID21-CZ.02.1.01/0.0/0.0/16_019/0000760). J.V. was partially supported by the Grant Agency of the Czech Technical University in Prague (Project No. SGS16/244/OHK4/3T/14). The study was also partially funded by RFBR (Project No. 18-33-20214) and JSPS KAKENHI Grants No. JP15K14133 and No. JP16H04501.

[1] G. Zhang, S. Dong, Z. Yan, Y. Guo, Q. Zhang, S. Yunoki, E. Dagotto, and J.-M. Liu, Phys. Rev. B **84**, 174413 (2011).

[2] R. D. Johnson, L. C. Chapon, D. D. Khalyavin, P. Manuel, P. G. Radaelli, and C. Martin, Phys. Rev. Lett. **108**, 067201 (2012).

[3] N. Perks, R. Johnson, C. Martin, L. Chapon, and P. Radaelli, Nat. Commun. **3**, 1277 (2012).

[4] J. T. Zhang, X. M. Lu, J. Zhou, H. Sun, F. Z. Huang, and J. S. Zhu, Phys. Rev. B **87**, 075127 (2013).

[5] X. Z. Lu, M.-H. Whangbo, S. Dong, X. G. Gong, and H. J. Xiang, Phys. Rev. Lett. **108**, 187204 (2012).

[6] K. Cao, R. D. Johnson, N. Perks, F. Giustino, and P. G. Radaelli, Phys. Rev. B **91**, 064422 (2015).

[7] J. S. Lim, D. Saldana-Greco, and A. M. Rappe, Phys. Rev. B **97**, 045115 (2018).

[8] A. A. Belik, Y. S. Glazkova, Y. Katsuya, M. Tanaka, A. V. Sobolev, and I. A. Presniakov, J. Phys. Chem. C **120**, 8278 (2016).

[9] W. Sławiński, R. Przeniosło, I. Sosnowska, M. Bieringer, I. Margiolaki, and E. Suard, Acta Crystallogr., Sect. B: Struct. Sci. **65**, 535 (2009).

[10] W. Slawiński, R. Przenioslo, I. Sosnowska, and V. Petříček, Acta Crystallogr., Sect. B: Struct. Sci. **68**, 240 (2012).

[11] R. D. Johnson, D. D. Khalyavin, P. Manuel, P. G. Radaelli, I. S. Glazkova, N. Terada, and A. A. Belik, Phys. Rev. B **96**, 054448 (2017).

[12] N. Terada, Y. S. Glazkova, and A. A. Belik, Phys. Rev. B **93**, 155127 (2016).

[13] F. Kadlec, V. Goian, C. Kadlec, M. Kempa, P. Vaněk, J. Taylor, S. Rols, J. Prokleška, M. Orlita, and S. Kamba, Phys. Rev. B **90**, 054307 (2014).

[14] M. N. Iliev, V. G. Hadjiev, M. M. Gospodinov, R. P. Nikolova, and M. V. Abrashev, Phys. Rev. B **89**, 214302 (2014).

[15] A. Nonato, B. Araujo, A. Ayala, A. Maciel, S. Yanez-Vilar, M. Sanchez-Andujar, M. Senaris-Rodriguez, and C. Paschoal, Appl. Phys. Lett. **105**, 222902 (2014).

[16] S. M. Souliou, Y. Li, X. Du, M. Le Tacon, and A. Bosak, Phys. Rev. B **94**, 184309 (2016).

[17] X. Du, R. Yuan, L. Duan, C. Wang, Y. Hu, and Y. Li, Phys. Rev. B **90**, 104414 (2014).

[18] C. Toulouse, C. Martin, M.-A. Measson, Y. Gallais, A. Sacuto, and M. Cazayous, Phys. Rev. B **99**, 024303 (2019).

[19] S. Skiadopoulou, V. Goian, C. Kadlec, F. Kadlec, X. F. Bai, I. C. Infante, B. Dkhil, C. Adamo, D. G. Schlom, and S. Kamba, Phys. Rev. B **91**, 174108 (2015).

[20] Y. S. Glazkova, N. Terada, Y. Matsushita, Y. Katsuya, M. Tanaka, A. V. Sobolev, I. A. Presniakov, and A. A. Belik, Inorg. Chem. **54**, 9081 (2015).

[21] M. Retuerto, S. Skiadopoulou, F. Borodavka, C. Kadlec, F. Kadlec, J. Prokleška, Z. Deng, J. A. Alonso, M. T. Fernandez-Diaz, F. O. Saouma *et al.*, Phys. Rev. B **97**, 144418 (2018).

[22] See Supplemental Material at http://link.aps.org/supplemental/10.1103/PhysRevB.99.184108 for additional details about the temperature dependence of the THz, IR, and Raman spectra.

[23] E. D. Palik and E. J. Prucha, *Handbook of Optical Constants of Solids* (Academic, Boston, MA, 1997).
[24] D. Rousseau, R. P. Bauman, and S. Porto, J. Raman Spectrosc. **10**, 253 (1981).
[25] A. Cracknell, J. Phys. C **2**, 500 (1969).
[26] R. Przenioslo, I. Sosnowska, E. Suard, A. Hewat, and A. Fitch, J. Phys.: Condens. Matter **14**, 5747 (2002).
[27] D. Nuzhnyy, J. Petzelt, V. Bovtun, M. Kempa, S. Kamba, J. Hlinka, and B. Hehlen, Phys. Rev. B **96**, 174113 (2017).